

Fabrication, Thermo-Mechanical, and Morphological Characterization of Hydroxyapatite-Reinforced Polyurethane Biocomposites as Dye Adsorbent for Effluent

Nida Mumtaz, Nadia Akram,* Khalid Mahmood Zia, Muhammad Saeed, and Muhammad Usman



Cite This: *ACS Omega* 2023, 8, 33310–33320



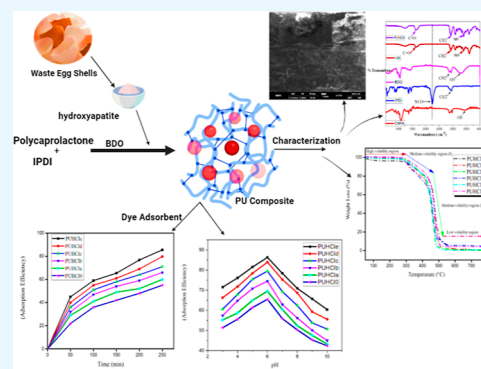
Read Online

ACCESS |

Metrics & More

Article Recommendations

ABSTRACT: Petrochemical costs, limited fossil fuel reserves, and concerns about greenhouse gas emissions have raised interest in developing renewable approaches for synthesizing biobased polyurethanes. This study aims to solve these problems by making nanocrystalline hydroxyapatite (HA) reinforcement from waste chicken eggshells and adding it to polyurethane synthesis through in situ polymerization. The novelty of the research lies in the utilization of HA as a reinforcement material and renewable resources for polyurethane production. The results confirm that HA was successfully added to the polyurethane backbone. Fourier transform infrared (FTIR) analysis confirmed that the NCO groups were changed to urethane linkages. TGA examination demonstrated that the samples exhibited thermal stability up to 457 °C with a mass loss of 61%, indicating enhanced thermal stability. DMA measurements showed improved mechanical properties of the synthesized polyurethanes, with storage modulus (E'), complex modulus (E^*), and compliance complex (D^*) values of 0.177, 22.522, and 0.660 MPa^{-1} , respectively. SEM analysis confirmed the homogeneous surface and well-dispersed HA reinforcement. Swelling characteristics revealed an optimum absorption of 30% H_2O , 35% CH_3OH , and 45% CCl_4 . Polyurethane composites exhibited significant chemical resistance and hydrolytic stability in acidic and basic media. Additionally, the composites demonstrated efficient adsorption of methyl orange from wastewater, with the PUHCl series achieving a maximum adsorption capacity of 85.50 mg/g under optimal conditions of 0.030 g/mL dose, 45 °C temperature, 2.5 h contact time, and pH 6.0..



1. INTRODUCTION

Rapid industrialization harms human health and the environment.¹ The use of toxic chemicals will increase because of economic growth. Safe use and disposal of toxic chemicals are essential.² Dye waste is produced in various industries, including cosmetics, food, paper, pharmaceuticals, plastics, textiles, and tanneries.³ In addition to harming human health, dye molecules disrupt aquatic and floral environments.⁴ Dye molecules contain chromogen-chromosphere structures that make them difficult to biodegrade.⁵ 80% of all dye production belongs to the textile industry, which uses it primarily.⁶ Due to their high corrosiveness, dyestuffs must be treated before discharge.⁷

In the past, dye waste has been treated in many ways. These include coagulation–flocculation,⁸ biodegradation,⁹ electrochemical oxidation,¹⁰ ion exchange,¹¹ Fenton oxidation, reverse osmosis, ozonation, electrocoagulation, and adsorptive treatments.¹² Social pressure is mounting on researchers to develop environmentally friendly and economically efficient techniques.¹³ Physical or chemical forces bind particles to the adsorbent during adsorption.¹⁴ In addition to metal oxides,

waste products are also utilized as adsorbents. Activated carbon is widely used. It is, however, uneconomical.¹⁵

Many researchers are now exploring waste materials as adsorbents and precursors.¹⁶ Waste materials are economically viable, abundantly available, eco-friendly, and chemically and mechanically stable.¹³ However, despite their favorable properties, waste-derived adsorbents typically have low adsorption capacities.¹⁷ Recent research focuses on developing environmentally friendly and low-cost adsorbent materials.¹⁸

Eggshell waste conversion into valuable commercial products is economically viable.¹⁹ Eggshell waste consists of many inorganic and organic components that can be utilized in numerous applications.²⁰ They can be used as reinforcements in thermoplastics. Biomaterials incorporating egg and food residues have various applications. The adsorption of organic

Received: April 8, 2023

Accepted: August 16, 2023

Published: September 7, 2023



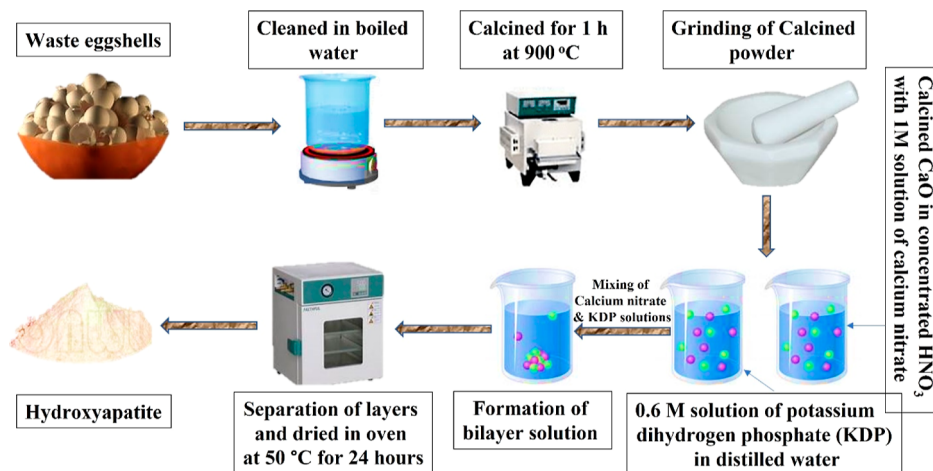


Figure 1. Synthesis of hydroxyapatite from waste chicken eggshells.

dyes and heavy metals makes such biomaterials remarkable in their sorption properties. Furthermore, these biomaterials are used in bioceramic production as calcium sources, and their properties as composite fillers are excellent.²¹

Recently, researchers showed interest in hydroxyapatite (HA) and its derivatives as alternative adsorbents for treating wastewater containing dyes and heavy metals.²² Their unique properties and structures also offer ion exchange capabilities, low solubility in water, high thermostability, and broad adsorptive capabilities for a wide range of pollutants.²³

In the present work, eggshells were selected as suitable waste biomaterials for HA extraction. Furthermore, HA can be used as a reinforcement in biocomposites for dye adsorption from waste effluents. The structural, thermo-mechanical, and morphological properties of the newly developed biocomposites were characterized in terms of Fourier transform infrared (FTIR) spectroscopy, thermal gravimetric analysis (TGA), dynamic mechanical analysis (DMA), and scanning electron microscopy (SEM), respectively. The swelling behavior and chemical stability of the synthesized biocomposites were checked in the presence of different organic solvents, including primary and acidic solutions, respectively. On the other hand, the dye degradation properties of synthesized biocomposites were also determined in terms of pH and contact time by using a methyl orange dye solution with the help of a UV–visible spectrophotometer. The newly obtained polyurethane-based HA biocomposites offer several advantages for dye degradation due to their low cost and eco-friendly nature.

2. MATERIALS AND METHODS

2.1. Materials. The synthesis of reinforcement and composites was achieved by using the following materials: polycaprolactone diol, PCL 225 (molecular weight = 2000 g/mol), isophorone diisocyanate, IPDI (molecular weight = 222.29 g/mol), and 1,4-butane diols (BDO) (Sigma-Aldrich, St. Louis, MO, USA), which were vacuum oven-dried at 80 °C for 1 h. Nitric acid, potassium dihydrogen phosphate (KDP), and ammonia purchased from Sigma-Aldrich were also utilized. Solvents used in this research were acetone, CH₃OH, and CCl₄, obtained from Sigma-Aldrich. In this research, only analytical-grade chemicals were used.

2.2. Synthesis of Hydroxyapatite Reinforcement. The synthesis of HA from chicken eggshells, followed by minor modifications, is shown in Figure 1. Eggshells were obtained

from an egg processing plant (Madina Egg Tray Factory, Faisalabad, Pakistan). Eggshells were cleaned in boiling water and calcined for 1 h at 900 °C in an electric furnace. The calcined powder was crushed using an alumina mortar and pestle. The resultant powder contains pure calcium oxide. After that, a 1 molar (M) calcium nitrate solution was prepared by adding calcined CaO to concentrated HNO₃ and diluting it with distilled water.²⁴ A 0.6 M KDP solution was also prepared in distilled water. Then a KDP solution was gradually added to the calcium nitrate solution. Ammonia was used to maintain the pH level at 10. This solution was vigorously stirred for 1 h and left to stand overnight at room temperature. As a result, a bilayer solution was obtained.²⁵ The top layer of the solution was clear ammonia, and white precipitates were collected at the bottom of the beaker. The collected precipitates were washed repeatedly with distilled water to eliminate NH₄⁺ and NO₃⁻ ions. The precipitates were filtered and dried in an oven at 50 °C for 24 h using filter paper. The resultant cake was then calcined in an electrical furnace for 30 min at 900 °C, employing a heating rate of 10 °C/min.²⁶

2.3. Fabrication of Polyurethane Composites. In situ polymerization was used to produce polyurethane composites.²⁷ A four-neck round-bottom flask was utilized in this procedure. The flask was fitted with a thermometer, an N₂ gas supply, a mechanical stirrer, and a condenser for reflux. During the reaction, a nitrogenous atmosphere was maintained by controlling bubbles of 10–12 μm per minute in a pyrogallol solution.²⁸ The reaction temperature was maintained in an oil bath during the entire process. In the first step, a calculated amount of PCL was added to the flask. Then the reaction temperature was increased to 60 °C. In the second step, the calculated quantity of diisocyanate was introduced dropwise to macrodiol, and the reaction mixture's temperature was raised to 100 °C. After 1 h of constant stirring, a polyurethane prepolymer with NCO terminal groups was developed. In the next step, the required quantity of chain extender BDO was added, and the reaction continued following vigorous stirring. The chain termination reaction continued for 20 min, and 15 wt % acetone was used to achieve homogeneity.

Polymerized polyurethane was obtained as a blank sample by reducing the reaction mixture temperature. Polyurethane composites were manufactured by adding measured amounts of HA reinforcement. Hard segment content varied from 5 to 30 wt % owing to changing the concentration of HA from 1 to

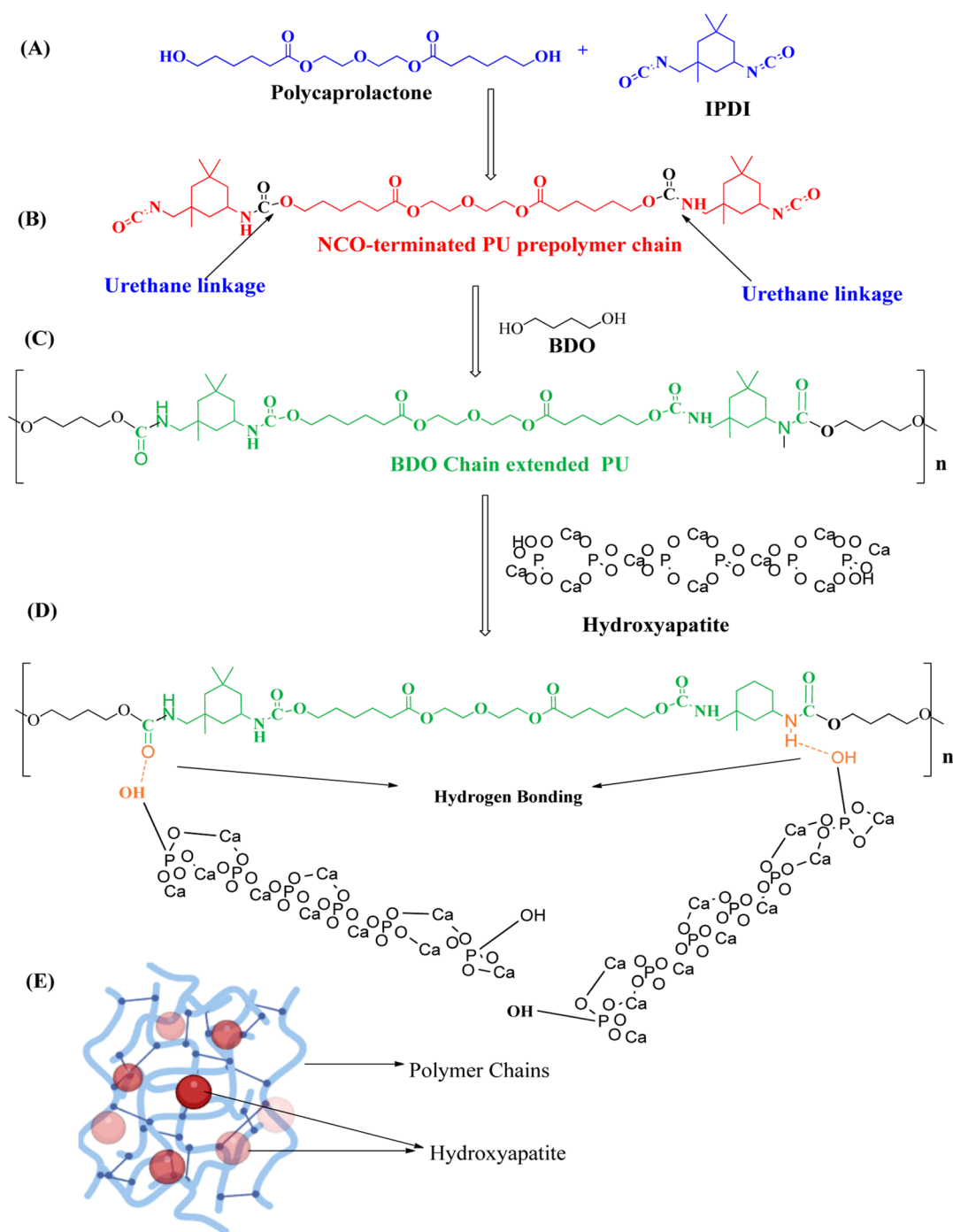


Figure 2. Synthetic strategy of polyurethane and its composites of the PUHCl series (A) monomer addition (B) development of NCO-terminated PU prepolymer chains (C) BDO-extended polyurethane (D) development of hydroxyapatite nanocomposites (E) morphology of hydroxyapatite nanocomposites.

3 wt %. HA was introduced into the reaction mixture according to the selected fabrication conditions. The following conditions were controlled during the reaction including stirring speed, temperature, and the synthesis atmosphere. A mechanical stirrer was used to ensure homogeneous filler (HA) mixing with the PU prepolymer at 1300 rpm. Polytetrafluoroethylene (PTFE) molds were used to cast lightweight composite samples. The fabricated route for synthesizing polyurethane composites is illustrated in Figure 2. The composite films were dried in an oven at different time intervals and temperatures. The films were then dried at 70 °C for 36 h before drying at

110 °C for 4 h. The films were then kept in a desiccator at room temperature for subsequent examinations.²⁹ By following this method, six samples were fabricated. The samples also include a blank sample of the PU polymer without any reinforced material (PUHCl0). Table 1 summarizes the detailed information about the composition of the prepared PU samples.

A structural study of the produced composites was analyzed using FTIR spectroscopy; TGA was utilized to study the thermal behavior of prepared samples; DMA was employed for mechanical analysis; and SEM studies were employed for

Table 1. Stoichiometry and PU Sample Codes for Aliphatic Diisocyanate Polyurethane Composites Are Described in Detail

sample code ^a	mole ratio of PU samples	hydroxyapatite (wt %)	HS contents (wt %)	SS contents (wt %)
PUHC10	1:2:1	0	5.0	95.0
PUHC1a	1:2:1	1.0	10.0	90.0
PUHC1b	1:2:1	1.5	15.0	85.0
PUHC1c	1:2:1	2.0	20.0	80.0
PUHC1d	1:2:1	2.5	25.0	75.0
PUHC1e	1:2:1	3.0	30.0	70.0

^aIn the composition of the PUHC1 series, the ratio of NCO/OH, was sustained as 1. a = HS Content²⁸ = [(W_{IPDI/PCL} + W_{BD})/W_{Total}] × 100. b = SS Content = [100 - HS content (%)].

morphological analysis. NaOH and HCl were used to test the chemical stability. The swelling test determined water, CCl₄, and CH₃OH retention affinities.

2.4. Characterization. The following techniques were used to characterize the synthesized PU samples.

2.4.1. Fourier Transform Infrared Spectroscopy. The functional groups were verified by using spectra captured on a Fourier transform infrared spectrometer (NICOLET 6700 spectrometer, Waltham, MA, USA). FTIR was employed in the transmission mode range 4000–400 cm⁻¹ with 40 scans. Along with conventional information, the hydrogen bonding index (HBI) was calculated using the absorption regions for bonded and unbonded carbonyl groups, as shown in eq 1.

$$\text{HBI} = \frac{A_{c=o(\text{bonded})}}{A_{c=o(\text{free})}} \quad (1)$$

2.4.2. Thermal Gravimetric Analysis. A PerkinElmer (Waltham, MA, USA) thermogravimetric analyzer was utilized to execute the analysis. For the analysis, the heating ramp rate was carefully chosen as 10 °C min⁻¹ in the presence of a nitrogenous atmosphere, and 50 mL/min was the nitrogen flow rate. The 50–700 °C temperature range was selected for thermograms.

2.4.3. Dynamic Mechanical Analysis. DMA (Q800; TA Instruments, New Castle, DE, USA) was used to record the values in the mode of temperature sweep with a temperature range of 200–1370 °C, a heating rate of 10 °C/min, and a frequency of 0.01–150 Hz. The values are compliance complex (*D**), complex modulus (*E**), and storage modulus (*E'*).

2.4.4. Scanning Electron Microscopy. The samples' surface morphology was performed using a JEOL JSM-7000F, California, USA. Twenty kV was applied as an accelerating voltage with a 9.0 ± 0.5 mm distance.

2.4.5. Swelling Test. Distilled water, CCl₄, and CH₃OH were used to evaluate the swelling behavior. Small samples from the polyurethane composites were immersed in these three solvents. In this way, weight change was evaluated until we observed a constant weight. To calculate the percentage of H₂O/CCl₄/CH₃OH consumption by the samples of polyurethane composites, eq 2 was used.

$$\begin{aligned} &\% \text{ age of H}_2\text{O/CCl}_4\text{/CH}_3\text{OH absorption} \\ &= \frac{\text{wet weight} - \text{Dry weight}}{\text{Total weight}} \times 100 \end{aligned} \quad (2)$$

2.4.6. Chemical Stability Test. PU samples were evaluated by immersing them in NaOH and HCl solutions, and then chemical resistance was evaluated.

2.4.7. Dye Adsorption Experiment. The adsorption performance of PU composites was assessed by using methyl orange as the model dye. The PU composite was dissolved in 10 mL of a methyl orange solution (100 mg/L). Adsorption occurs after a certain period. Centrifugation was used to separate the supernatant solutions. Measurements were taken by using a UV–visible spectrophotometer. The wavelength was set to 464 nm. The adsorption efficiency of methyl orange on PU composite was computed by using the following eq 3.

$$D = \frac{C_o - C_t}{C_o} \times 100\% \quad (3)$$

where *C*_o is the initial concentration of dye and *C*_{*t*} is the concentration at time *t* (mg/L).

3. RESULTS AND DISCUSSION

3.1. FTIR Characterization. Four types of materials were analyzed using FTIR spectroscopy: PU monomers (PCL, IPDI, and BDO), reinforcement (HA), and the resultant polyurethane-based HA biocomposites. The FTIR peaks of the synthesized biocomposites are summarized in Table 2. The

Table 2. Fourier Transform Infrared (FTIR) Spectra of Polyurethane Were Calculated According to Wave Numbers (cm⁻¹)

assignments	wave number (cm ⁻¹) observed value	literature value ^{30–32}
C=O stretching	1611, 1700	1728, 1725
symmetric and asymmetric stretching of CH ₂ group	2950, 2830	2940, 2850
NH stretch	3390	3400
urethane C=O bands	1700	1700
OH	3600	3565
H ₂ O	3420, 1640	3441, 1645
-PO ₄ ³⁻	1080, 1010	1094, 1035

FTIR spectra showed peaks of symmetric and asymmetric vinyl linkages and carbonyl and amide linkages, as shown in Figure 3A,B, respectively. Figure 3A shows a strong peak between 1615 and 1720 cm⁻¹, indicating the carbonyl group (C=O) stretching of the soft segment of PCL and the stretching modes of the C=C and C=O functional groups of carboxylic acid and carbonyls, respectively. Peaks at 2922 and 2850 cm⁻¹ indicated symmetric and asymmetric stretching of the CH₂ group. There was a strong peak at 2233.66 cm⁻¹ due to certain isocyanate (-NCO) groups of isophorone diisocyanate (IPDI). IPDI exhibited C–H stretching peaks at 2940 cm⁻¹.

Peaks at 3400 cm⁻¹ correspond to the NH stretch, while urethane C=O bands are observed in the 1700 cm⁻¹ region. The HA spectrum exhibits the presence of OH, H₂O, and PO₄³⁻ at 3565, 3441, 1645, 1094, and 1035 cm⁻¹, respectively. The phosphate radical bands (PO₄³⁻) of HA are observed at 1094 and 1035 cm⁻¹. Figure 3B indicates that none of the prepared samples exhibit the NCO group peak at 2250–2500 cm⁻¹, suggesting that all NCO groups were converted to urethane linkages during chain extension. It demonstrates a complete reaction between the hydroxyl and isocyanate groups. The HBI values were evaluated using FTIR spectra and are expressed in Table 3. Figure 3C shows the hydrogen-

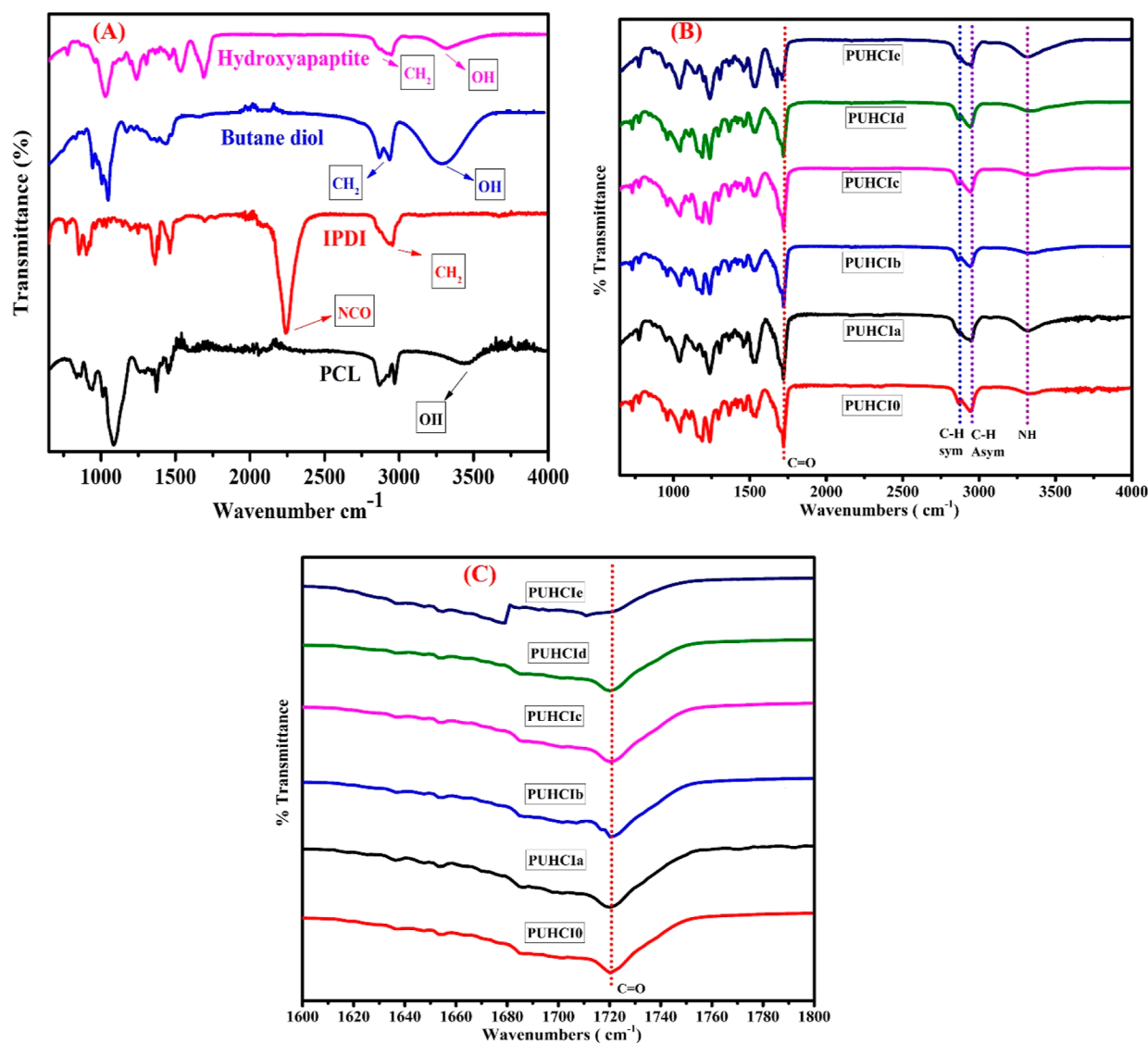


Figure 3. (A) FTIR spectra of monomers, reinforcement, and polymers: PCL (macrodiol), IPDI (isocyanates), BDO (chain extender), HA (reinforcement), (B) FTIR spectra of PUHCl-based biocomposites films. (C) FTIR spectra of PU elastomers showing a hydrogen-bonded carbonyl region and a free carbonyl region.

Table 3. Evaluation of Polyurethane Elastomers Hydrogen Bonding Index

sample code	$A_{\text{C=O(bonded)}}$	$A_{\text{C=O(free)}}$	HBI ^{33,34}
PUHCl0	4.35	4.38	0.99
PUHClA	3.62	3.49	1.03
PUHClB	2.83	2.69	1.05
PUHClC	2.02	1.84	1.09
PUHClD	1.21	1.05	1.14
PUHClE	0.47	0.31	1.51

bonded C=O and free C=O stretching vibrational modes in the FTIR peaks that were used to determine this parameter. “HS” acts as a proton acceptor for urethane linkages with polar carbonyl groups. The HBI is an authentic parameter for understanding hydrogen bonds by analyzing urethane carbonyl stretching peaks. It appears that two carbonyl stretching regions contribute to this phenomenon. The first band is observed around 1720–1719 cm⁻¹ due to free urethane carbonyl groups stretching. The second band is observed

around 1710–1712 cm⁻¹ due to hydrogen-bonded carbonyl groups in urethane bonds. The frequencies of the carbonyl-free groups shift downward. Polyurethanes contain proton donors such as urea, amide, and urethane. Dissociation of hydrogen bonds occurs at the interface and in reaction mixtures between “HS” and “SS.”

A carbonyl oxygen proton acceptor in the urethane group produces two absorption bands, which separate HS from SS. The HBI is calculated as the ratio between these two peaks to estimate hydrogen bonding. Microphase separation was investigated by using FTIR by examining interchain hydrogen bonds. Measurements were made between 1800 and 1600 cm⁻¹ to determine the extent of hydrogen bonding. PU elastomers with a higher HBI value exhibit more hydrogen bonding between the carbonyl groups.

Consequently, the increase in “HS” has resulted in a significant increase in urethane linkages, which are located and contribute to hydrogen bonding because of a more significant number of carbonyl groups. Hydrogen bonding is a type of dipole–dipole interaction between the lone pair of a highly

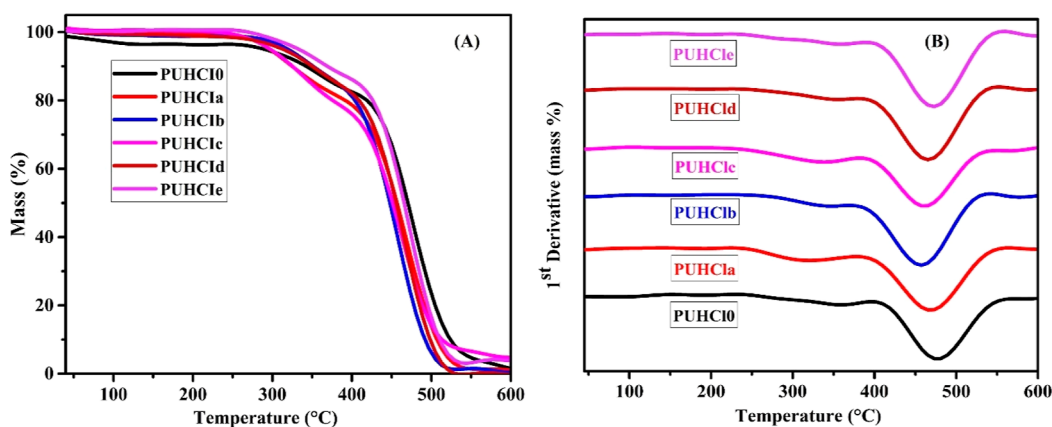


Figure 4. (A) TGA curves of hydroxyapatite-based biocomposites and (B) DTG curves of hydroxyapatite-based biocomposites

electronegative atom (typically N, O, or F) and the hydrogen atom in an N–H, O–H, or F–H bond. The formation of hydrogen bonds is an essential quality of liquid water that is crucial to life as we know it. In liquid water, hydrogen bonds are constantly formed and broken as the water molecules slide past each other. Ice is less dense than water because the orientation of hydrogen bonds causes molecules to push farther apart, which lowers the density.

3.2. TGA Assessment of Thermal Stability. Figure 4A,B illustrates the TG and DTG curves for PUHC10 and its composite materials containing 1.0, 1.5, 2.0, 2.5, and 3.0 wt % HA reinforcement (PUHC1a, PUHC1b, PUHC1c, PUHC1d, and PUHC1e, respectively). Table 4 shows each degradation

Table 4. Percentage of Mass Loss for Polyurethane (PU) Composites Determined by Thermal Gravimetric Analysis (TGA) and Their First Derivative Analysis (DTG)

sample codes	stage I			stage II		
	T_{Onset} (°C)	T_{max}^a (°C)	mass loss (%)	T_{Onset} (°C)	T_{max}^a (°C)	mass loss (%)
PUHC10	249	354	12	410	473	53
PUHC1a	241	306	7	394	465	46
PUHC1b	249	330	9	386	449	33
PUHC1c	241	322	8	394	457	39
PUHC1d	249	338	10	402	457	39
PUHC1e	241	346	11	402	457	39

^a T_{max} = temperature of maximum degradation rate.

stage's corresponding degradation temperatures and mass losses. The results of both studies indicate that PUHC1d and PUHC1e are thermally more stable than PUHC1a, PUHC1b, and PUHC1c, respectively. The thermal stability of PUs is expected to improve when reinforced with HA, particularly during the first decomposition phase. Two stages are involved

in the decomposition of composites.³⁵ This first step of decomposition, with T_{max} of 306, 330, 322, 338, and 346 °C for PUHC1a, PUHC1b, PUHC1c, PUHC1d, and PUHC1e, illustrates the breakdown of urethane groups of PU (matrix) and calcium and phosphate from HA (reinforcement). The second phase of decomposition, which occurs at $T_{\text{max}} \sim 457$ °C in all composites, corresponds to the breakdown of the structural bonds between the hydroxyl chains of HA.

3.3. DMA Analysis. Dynamic mechanical analysis is a versatile technique commonly used to obtain a comprehensive mechanical profile of composites. In the case of polyurethane composites, a detailed mechanical description can be derived from the storage modulus information, which is presented in Table 5. The storage modulus (E') provides insights into the reserved elastic energy and can track even slight composition changes. By studying parameters such as the storage modulus, complex modulus (E^*), complex compliance (D^*), and chain entanglement (N), a better understanding of composite behavior can be achieved, mainly when different reinforcement concentrations are employed. The interfacial adhesion between the matrix and reinforcing agents plays a crucial role in the mechanical properties of composites. In the case of HA-filled composites, Figure 5A demonstrates different temperature dependences on E' . The storage modulus values decrease with increasing temperature due to the continuous relaxation of the chains. The increase in "HS" (hydrogen bonding sites) leads to a significant increase in urethane linkages, contributing to hydrogen bonding through more carbonyl groups.

Figure 5A exhibits an obvious decrease in response to variations in the HS and HA contents. The storage modulus (E') indicates molecular relaxation and material stiffness. However, the E' values of the composites with soft and flexible segments did not reach the anticipated levels. The PU blanks and composites filled with HA at lower concentrations displayed minimal variation, with levels gradually increasing.

Table 5. Mechanical Profile of Polyurethane Composite

sample code	HS (wt %)	SS (wt %)	HA (wt %)	E' (MPa)	E^* (MPa)	D^* (1/MPa)	$N \times 10^{-4}$ (mol m ⁻³)
PUHC10	5.0	95.0	0	0.093	15.154	0.422	0.625
PUHC1a	10.0	90.0	1.0	0.107	16.930	0.485	0.719
PUHC1b	15.0	85.0	1.5	0.137	21.024	0.585	0.921
PUHC1c	20.0	80.0	2.0	0.163	24.176	0.700	0.109
PUHC1d	25.0	75.0	2.5	0.215	26.176	0.853	0.144
PUHC1e	30.0	70.0	3.0	0.352	31.672	0.914	0.236

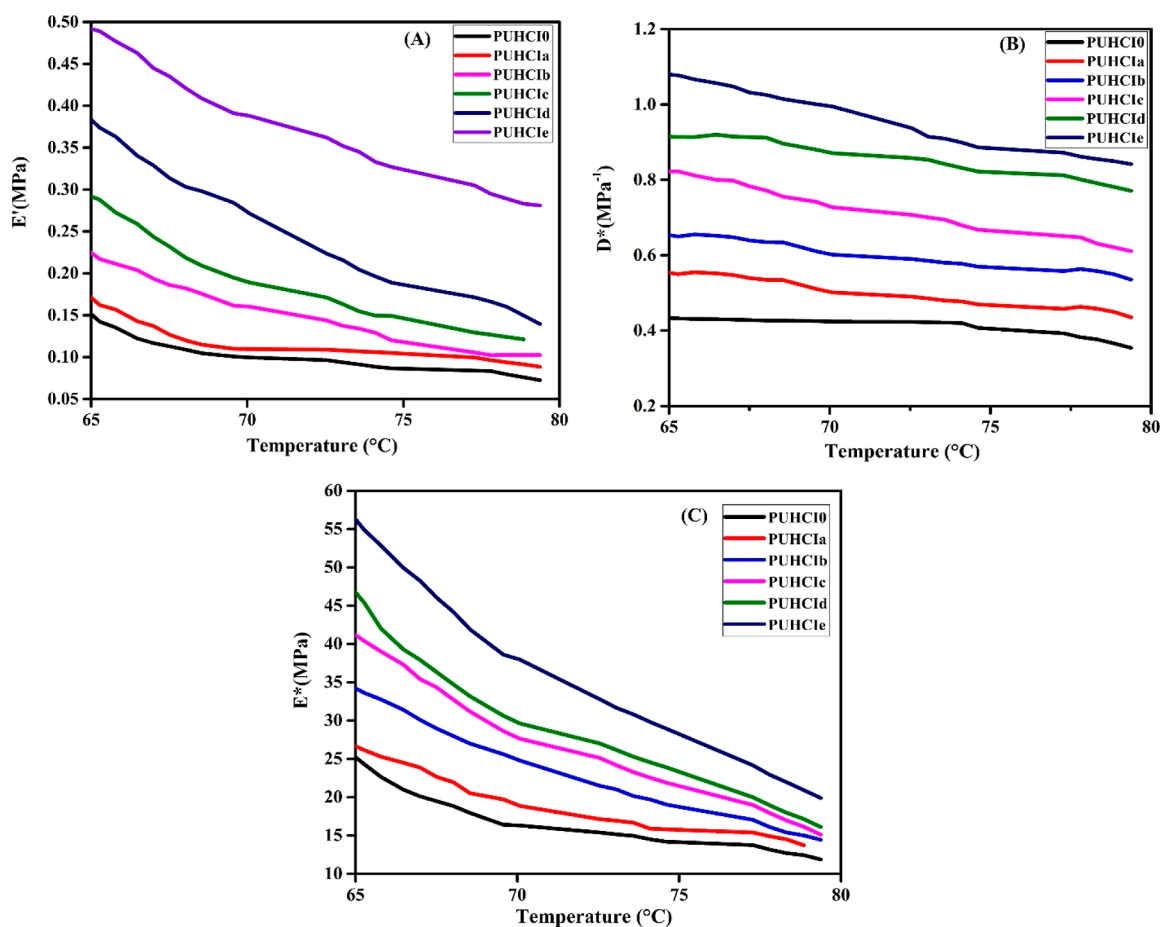


Figure 5. Mechanical behavior of the polyurethane composite. (A) Storage modulus and temperature relationship. (B) Compliance complex and temperature relationship. (C) Relationship between complex modulus and temperature.

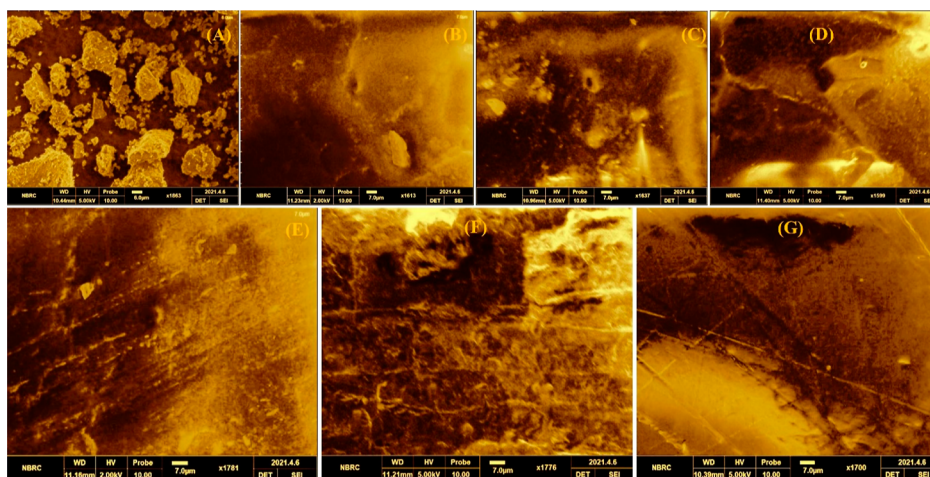


Figure 6. SEM image of PU composite (A) SEM of hydroxyapatite reinforcement (B) SEM of PUHC10 (C) SEM of PUHC1a (D) SEM of PUHC1b (E) SEM of PUHC1c (F) SEM of PUHC1d (G) SEM of PUHC1e.

The addition of fillers introduced numerous functionalized groups to the composites. The polymer matrix formed strong bonds susceptible to cleavage with increasing temperature, resulting in a decrease in E' . Higher E' values indicate effective dispersion of reinforcement.³⁶ Figure 5C illustrates the viscoelastic characteristics of polymers and composites as represented by the complex modulus (E^*). Equation 4 elaborates the description of E^* as a combination of the

elastic modulus (E') as well as the loss modulus E'' . Its E^* values can determine the stiffness of a material.

$$E^* = E' + iE'' \quad (4)$$

Figure 5C depicts the dependency of the dynamic modulus, or complex modulus (E^*), on various factors. The trend that is given by the storage modulus is followed by the complex modulus (E^*). HA used as a filler shows a positive effect on E^*

in the presence of aliphatic diisocyanate, thus verifying the results of (E'). All composite samples were also assessed using complex compliance (D^*) for their viscoelastic behavior (Figure 5B). Complex compliance, on the other hand, is known as creep compliance. The viscoelastic behavior of polyurethane composites with HA was investigated, and it was found that the sample strength increased with temperature.

The mechanical performance of polyurethane composites with HA varied slightly, and the addition of HA stabilized the composites, which was sufficient for some applications. However, increasing the hard segment (HS) content could only make significant changes. The soft segment (SS) PCL was found to lower the mechanical strength, and the degree of entanglement density (N) was calculated using eq 5 to understand PCL behavior as SS. The reticular structure produced in the polymer matrix at cross-linking points was either coiled or globular in shape, and it strongly influenced polymer rheology, which played a significant role in the process.³¹ DMA measurements with E' were used to calculate this factor, where R and T are gas constants and temperatures, respectively.

$$N = \frac{E'}{6RT} \quad (5)$$

Table 5 indicates a low cross-link density, implying insufficient entanglement between the molecular chains to produce significant stiffness, even with reinforcement. The study also revealed that the matrix and filler did not interact chemically, and the matrix and filler exhibited physical cross-linking.

3.4. Morphology of Hydroxyapatite-Induced PU Composites by SEM. Figure 6A displays a micrograph of n-HA reinforcement, which shows that the particle's surface has an uneven and porous structure, leading to a larger specific surface area of HA. Due to its pores, it disperses across solid surfaces, and no eggshell membrane was present on the particle's surface, indicating that the eggshell membrane had been removed.³⁷ Different micrographs of PU-reinforced composites are shown in Figure 6, revealing a sheet-like or flat structure. Some points in the morphological images show uneven or coarse surfaces because they are covered with crinkles, indicating the presence of defects in the structure. These micrographs showed that reinforcement HA was embedded in the PU matrix, and they further indicated a deficient concentration of polymer chain entanglements.

Consequently, all components were evenly distributed, preventing bulging. Figure 6C,D,F shows some transparent spots in the morphology, while others 6B,E,G emerge as waves, suggesting that HA reinforcement was present in the form of monolayers. HA was uniformly distributed throughout all samples in SEM images at varying magnifications, indicating considerable hydrogen bonding due to the incorporation of HA in the PU matrix. The interactions between PU and HA were visible, and the reinforcement was visible in all of the morphological images. The micrographs were rough, and the edges revealed the oxygen attachment to the HA, forming strong bonds between the defective HA sites and oxygen. Regardless of the filler amount, the composites exhibited a uniform dispersion of HA fillers.³²

3.5. Swelling Characteristics of Hydroxyapatite-Induced PU Composites. Different solvents exhibit varying swelling behaviors in polymers, which is a complex phenomenon that has been extensively studied statistically.

Understanding swelling behavior is crucial because, in materials, interactions with solvents are inevitable. Water is considered a universal solvent and has a high composite water absorbance capacity. However, most organic solvents, such as CH_3OH and CCl_4 , partially or entirely dissolve polymer networks. CH_3OH is a protic solvent like H_2O , while CCl_4 is an aprotic solvent. CCl_4 has a broad spectrum of solvent compatibilities and can dissolve polar and nonpolar substances. It is also suitable for dissolving polyurethane. Figure 7

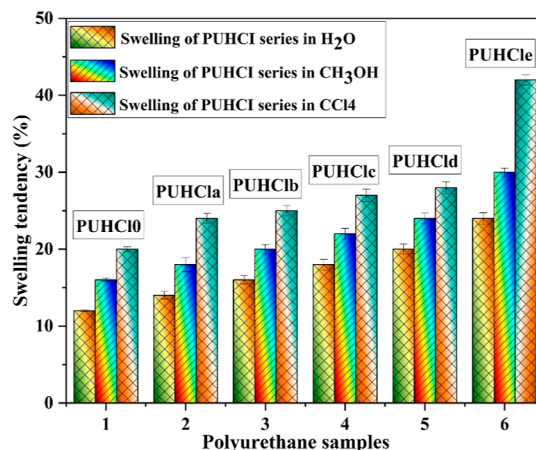


Figure 7. Swelling behavior of PUHCl series in H_2O , CH_3OH , and CCl_4 .

illustrates the swelling behavior of the PUHCl chains in H_2O , CH_3OH , and CCl_4 . It shows that PU samples synthesized from aliphatic diisocyanates have a higher affinity for protic solvents. It could be attributed to aromatic isocyanates producing more cross-linking, which hinders solvent penetration. The greater the $\text{H}_2\text{O}/\text{CH}_3\text{OH}$ penetration, the lower the solvent swelling contents. This phenomenon in polyurethane composites reflects phase segregation, which is more pronounced in HA. However, the swelling tendency of the polymer in CCl_4 is a complex manifestation. The composite exhibits a significant increase in swelling compared to H_2O and CH_3OH , which can be attributed to its CCl_4 nature. Precise observations indicate that CCl_4 absorbs 45% higher than water and methanol.³⁸ There is also the possibility of a continuous swelling reduction. The fundamental reason for the deformation of the PU composite's structure is the breaking of secondary bonding after absorbing a certain quantity of solvent. Instead of maintaining the sample's structure, the exposed material dissolves in the solvent because its original weight cannot be sustained in the solvent.³⁹

3.6. Chemical Stability of Hydroxyapatite-Induced PU Composites. The chemical resistance of the prepared HA-based biocomposites was tested against NaOH and HCl solutions for 100 h and is represented in Table 6. In the case of PUHCl0, the sample was completely affected. Excellent chemical resistance was observed from PUHCl0 to PUHCl6 of the prepared HA-based biocomposites against the HCl solution. Biocomposites reported slightly inferior chemical resistance to an alkaline medium (NaOH) than to an HCl solution. Ester bond hydrolysis may affect biocomposite adhesion.⁴⁰

3.7. Dye Degradation. In this study, the impact of time and pH on the adsorption capability of the methyl orange dye

Table 6. Chemical Stability Profile of Polyurethane Composite

serial no	sample code	chemical resistance ^a	
		HCl (6%) for 100 h	NaOH (6%) for 100 h
1	PUHC10	A	a
2	PUHC1a	B	a
3	PUHC1b	C	d
4	PUHC1c	C	d
5	PUHC1d	C	d
6	PUHC1e	C	e

^aa = Film completely affected. b = Film completely removed. c = Film partially removed. d = Slight loss in glass. e = unaffected.

solution was investigated. The maximum wavelength of the MO was 464 nm. The temperature was set to 45 °C.

3.7.1. Effect of pH on the Adsorption Efficiency of MO Solution. The measurement of pH is a crucial parameter in adsorption studies. Methyl orange, a standard laboratory indicator, changes color in response to variations in pH. The present study used a fixed dose of 0.030 g/mL of PU composite, and the temperature was maintained at 45 °C. The adsorption process was completed in 10 h, and the concentration of MO was 100 mg/L. The impact of pH on adsorption efficiency is illustrated in Figure 8B. The results indicate that an increase in pH from 3 to 6 leads to a noticeable improvement in the adsorption efficiency. It is because the surface of the PU composite has a hydroxyl group, which gets protonated and forms hydrogen bonds with the N atoms of the MO skeleton. The SO₃ group in the methyl orange molecule also creates electrostatic adsorption with the hydroxyl proton, which makes the adsorption work better. However, the adsorption effectiveness decreases when the pH increases from 7 to 10. Alkaline conditions make it hard to form hydrogen bonds, which makes it hard for PU composites to attract MO molecules with electrostatic forces.⁴¹ In an acidic environment, methyl orange exists in the Quindo form and rearranges itself into an azo structure as the pH values increase. Therefore, the highest adsorption efficiency occurs at a pH of 6.⁴²

3.7.2. Effect of Contact Time on the Adsorption Efficiency of MO Solution. Figure 8A shows the effect of contact time on the adsorption efficiency of methyl orange solution under

certain conditions, such as a fixed dosage of PU composite (0.030 g/mL), a temperature of 45 °C, a concentration of 100 mg/L in the methyl orange solution, and a pH of 6.0. At the initial adsorption stage, the results show that adsorption efficiency rapidly increases with prolonged time, followed by a slow increase until reaching adsorption equilibrium, which occurs after 2.5 h. The rapid adsorption at the initial stage can be attributed to the attachment of methyl orange molecules to the composite surface, which provides more adsorption sites in the PU composite.⁴³ The adsorption equilibrium is achieved when the contact time exceeds 2.5 h, and as the contact time increases, the adsorption efficiency also tends to change to some extent. Experimental data indicate that 2.5 min is sufficient to achieve adsorption equilibrium.⁴⁴ Therefore, it can be concluded that the optimum contact time for adsorption is 2.5 h, as shown in Figure 8A.

4. CONCLUSIONS

In this study, aliphatic diisocyanate IPDI, biodegradable polyol PCL, and chain extender BDO are used to make biobased polyurethane composites with eggshell-derived HA as reinforcement. In the present work, a concentration of 1 to 3 (wt %) of HA was used. The prepared samples were characterized using conventional techniques, including FTIR, TGA, DMA, and SEM. The FTIR study provided evidence of the development of the urethane linkage through the appearance of the amide group peak and the disappearance of the NCO peak. TGA was used to find out how stable the PU samples were at high temperatures, and it was found that the stability increased with the amount of HA up to 457 °C. The DMA study revealed that an increase in the HA content in the PU composite led to an increase in the stiffness of the polymer. All of the samples of PU composites exhibited consistency in behavior. DMA also showed a lower degree of entanglement (*N*), 0.459 mol m⁻³. SEM confirmed that the reinforced HA was well dispersed and that the surface of the produced samples was homogeneous. Strong segregation, which is a characteristic behavior of polyurethane, was detected. The swelling test assessed the penetration tendencies of various solvents, including H₂O, CH₃OH, and CCl₄. The results revealed that H₂O, CH₃OH, and CCl₄ exhibited penetration tendencies of 30, 35, and 45%, respectively. Polyurethane composites exhibited remarkable chemical

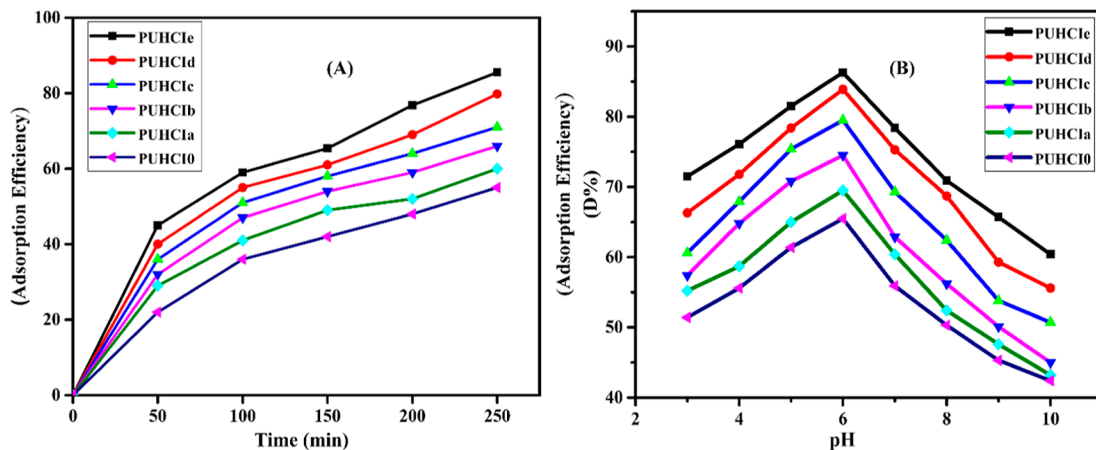


Figure 8. Adsorption efficiency (A) effect of contact time on the MO solution's adsorption effectiveness. (b) Effect of pH on the MO solution's adsorption effectiveness.

resistance and hydrolytic stability in acidic and salt solutions. The PU composite demonstrated an excellent capacity for the adsorption of methyl orange dye. However, further life cycle assessments or ecotoxicity studies will be necessary to determine whether these HA-based polyurethane biocomposites can be used as dye adsorbents with minimal environmental impact.

AUTHOR INFORMATION

Corresponding Author

Nadia Akram – Department of Chemistry, Government College University Faisalabad, Faisalabad 38000, Pakistan; orcid.org/0000-0002-4937-2409; Email: nadiaakram@gcu.edu.pk

Authors

Nida Mumtaz – Department of Chemistry, Government College University Faisalabad, Faisalabad 38000, Pakistan

Khalid Mahmood Zia – Department of Chemistry, Government College University Faisalabad, Faisalabad 38000, Pakistan

Muhammad Saeed – Department of Chemistry, Government College University Faisalabad, Faisalabad 38000, Pakistan; orcid.org/0000-0002-8759-6948

Muhammad Usman – Department of Chemistry, Government College University Faisalabad, Faisalabad 38000, Pakistan

Complete contact information is available at:

<https://pubs.acs.org/10.1021/acsomega.3c02371>

Notes

The authors declare no competing financial interest.

ACKNOWLEDGMENTS

The authors wish to express their profound gratitude to the International Foundation for Science (IFS) and the Organization for the Prohibition of Chemical Weapons (OPCW) for the research grant agreement no. I-2-F-6132-1 to complete this work.

REFERENCES

- (1) Shaltout, W. A.; El-Naggar, G. A.; Esmail, G.; Hassan, A. F. Synthesis and characterization of ferric@ nanocellulose/nanohydroxyapatite bio-composite based on sea scallop shells and cotton stalks: adsorption of Safranin-O dye. *Biomass Convers. Biorefin.* **2022**, 1–18.
- (2) You, Y.; Huang, Z.; Ma, R.; Shi, C.; Li, X.; Liu, D.; Dong, M.; Guo, Z. Sodium alginate templated hydroxyapatite/calcium silicate composite adsorbents for efficient dye removal from polluted water. *Int. J. Biol. Macromol.* **2019**, 141, 1035–1043.
- (3) Bhatt, P.; Joshi, S.; Urper Bayram, G. M.; Khati, P.; Simsek, H. J. E. R. Developments and application of chitosan-based adsorbents for wastewater treatments. *Environ. Res.* **2023**, 226, 115530.
- (4) Ragab, A.; Ahmed, I.; Bader, D. The removal of brilliant green dye from aqueous solution using nano hydroxyapatite/chitosan composite as a sorbent. *Molecules* **2019**, 24 (5), 847.
- (5) Al-Wafi, R.; Ahmed, M.; Mansour, S. Tuning the synthetic conditions of graphene oxide/magnetite/hydroxyapatite/cellulose acetate nanofibrous membranes for removing Cr (VI), Se (IV) and methylene blue from aqueous solutions. *J. Water Process Eng.* **2020**, 38, 101543.
- (6) Laabd, M.; Brahmi, Y.; El Ibrahim, B.; Hsini, A.; Toufik, E.; Abdellaoui, Y.; Abou Oualid, H.; El Ouardi, M.; Albourine, A. A novel mesoporous Hydroxyapatite@ Montmorillonite hybrid composite for high-performance removal of emerging Ciprofloxacin antibiotic from water: Integrated experimental and Monte Carlo computational assessment. *J. Mol. Liq.* **2021**, 338, 116705.
- (7) Khan, M.; Chowdhury, M.; Rahman, M. Biobased amphoteric aerogel derived from amine-modified clay-enriched chitosan/alginate for adsorption of organic dyes and chromium (VI) ions from aqueous solution. *Mater. Today Sustain.* **2021**, 13, 100077.
- (8) Ugbole, S. C.; Kim, Y. K.; Warner, S. B.; Fan, Q.; Yang, C. L.; Kyzymchuk, O.; Feng, Y.; Lord, J. The formation and performance of auxetic textiles. Part II: geometry and structural properties. *J. Text. Inst.* **2011**, 102 (5), 424–433.
- (9) Mustafa, G.; Tariq Zahid, M.; Ali, S.; Zaghum Abbas, S.; Rafatullah, M. Biodegradation and discoloration of disperse blue-284 textile dye by *Klebsiella pneumoniae* GM-04 bacterial isolate. *J. King Saud Univ. Sci.* **2021**, 33 (4), 101442.
- (10) Xia, Y.; Wang, G.; Guo, L.; Dai, Q.; Ma, X. Electrochemical oxidation of Acid Orange 7 azo dye using a PbO₂ electrode: Parameter optimization, reaction mechanism and toxicity evaluation. *Chemosphere* **2020**, 241, 125010.
- (11) M Nahiun, K.; Sarker, B.; N Keya, K.; I Mahir, F.; Shahida, S.; A Khan, R. A review on the methods of industrial waste water treatment. *Sci. Rev.* **2021**, 7 (73), 20–31.
- (12) Adnan, F. H.; Pons, M. N.; Mousset, E. Thin film microfluidic reactors in electrochemical advanced oxidation processes for wastewater treatment: A review on influencing parameters, scaling issues, and engineering considerations. *Electrochem. Sci. Adv.* **2023**, 3 (2), No. e2100210.
- (13) Mallakpour, S.; Behranvand, V. Waste-mediated synthesis of polymer nanocomposites and assessment of their industrial potential exploitations. *Handbook of Polymer Nanocomposites for Industrial Applications*; Elsevier, 2021; pp 147–167.
- (14) Bushra, R.; Mohamad, S.; Alias, Y.; Jin, Y.; Ahmad, M. J. M.; Materials, M. Current approaches and methodologies to explore the perceptive adsorption mechanism of dyes on low-cost agricultural waste: A review. *Microporous Mesoporous Mater.* **2021**, 319, 111040.
- (15) Moosavi, S.; Lai, C. W.; Gan, S.; Zamiri, G.; Akbarzadeh Pivezhzani, O.; Johan, M. R. Application of efficient magnetic particles and activated carbon for dye removal from wastewater. *ACS Omega* **2020**, 5 (33), 20684–20697.
- (16) Zia, Z.; Hartland, A.; Mucalo, M. R. Use of low-cost biopolymers and biopolymeric composite systems for heavy metal removal from water. *Int. J. Environ. Sci. Technol.* **2020**, 17, 4389–4406.
- (17) Tshikovhi, A.; Mishra, S. B.; Mishra, A. K. Nanocellulose-based composites for the removal of contaminants from wastewater. *Int. J. Biol. Macromol.* **2020**, 152, 616–632.
- (18) Anastopoulos, I.; Pashalidis, I. Environmental applications of Luffa cylindrica-based adsorbents. *J. Mol. Liq.* **2020**, 319, 114127.
- (19) Ghosh, S.; Pramanik, K. Unveiling the secrets of food waste derived biomaterials in remediation of environmental pollutants-A review. *Bioresour. Technol. Rep.* **2023**, 22, 101469.
- (20) Kalpana, M.; Nagalakshmi, R. Nano hydroxyapatite for biomedical applications derived from chemical and natural sources by simple precipitation method. *Appl. Biochem. Biotechnol.* **2023**, 195, 3994.
- (21) Nagalakshmi, R.; Kalpana, M.; Prabasheela, B. Eggshell derived calcium oxide-Synthesis and characterization. *AIP Conference Proceedings*; AIP Publishing LLC, 2022; Vol. 2446, p 130010.
- (22) Amenaghawon, A. N.; Anyalewechi, C. L.; Darmokoesomo, H.; Kusuma, H. S. Hydroxyapatite-based adsorbents: Applications in sequestering heavy metals and dyes. *J. Environ. Manage.* **2022**, 302, 113989.
- (23) Aaddouz, M.; Azzaoui, K.; Akartasse, N.; Mejdoubi, E.; Hammouti, B.; Taleb, M.; Sabbahi, R.; Alshahateet, S. Removal of Methylene Blue from aqueous solution by adsorption onto hydroxyapatite nanoparticles. *J. Mol. Struct.* **2023**, 1288, 135807.
- (24) Agbabiaka, O.; Oladele, I.; Akinwekomi, A.; Adediran, A.; Balogun, A. O.; Olasunkanm, O.; Olayanju, T. Effect of calcination temperature on hydroxyapatite developed from waste poultry eggshell. *Sci. Afr.* **2020**, 8, No. e00452.
- (25) Mohd Pu'ad, N.; Alipal, J.; Abdullah, H.; Idris, M.; Lee, T. Synthesis of eggshell derived hydroxyapatite via chemical precipitation and calcination method. *Mater. Today* **2021**, 42, 172–177.

- (26) Trakoolwannachai, V.; Kheolamai, P.; Ummartyotin, S. Development of hydroxyapatite from eggshell waste and a chitosan-based composite: In vitro behavior of human osteoblast-like cell (Saos-2) cultures. *Int. J. Biol. Macromol.* **2019**, *134*, 557–564.
- (27) Akram, N.; Zia, K. M.; Sattar, R.; Tabassum, S.; Saeed, M. Thermomechanical investigation of hydroxyl-terminated polybutadiene-based linear polyurethane elastomers. *J. Appl. Polym. Sci.* **2019**, *136* (13), 47289.
- (28) Akram, N.; Zia, K. M.; Saeed, M.; Usman, M.; Khan, W. G. Role of isophorone diisocyanate in the optimization of adhesion tendency of polyurethane pressure sensitive adhesives. *J. Appl. Polym. Sci.* **2019**, *136* (9), 47124.
- (29) Akram, N.; Zia, K. M.; Saeed, M.; Usman, M.; Saleem, S. Impact of macrodiols on the adhesion strength of polyurethane pressure-sensitive adhesives. *J. Appl. Polym. Sci.* **2018**, *135* (45), 46635.
- (30) Kumar, L.; Ahuja, D. Preparation and characterization of aliphatic polyurethane and modified hydroxyapatite composites for bone tissue engineering. *Polym. Bull.* **2020**, *77*, 6049–6062.
- (31) Du, J.; Zuo, Y.; Lin, L.; Huang, D.; Niu, L.; Wei, Y.; Wang, K.; Lin, Q.; Zou, Q.; Li, Y. Effect of hydroxyapatite fillers on the mechanical properties and osteogenesis capacity of bio-based polyurethane composite scaffolds. *J. Mech. Behav. Biomed. Mater.* **2018**, *88*, 150–159.
- (32) Mustafov, S. D.; Sen, F.; Seydibeyoglu, M. O. Preparation and characterization of diatomite and hydroxyapatite reinforced porous polyurethane foam biocomposites. *Sci. Rep.* **2020**, *10* (1), 13308.
- (33) Chen, C. P.; Dai, S. A.; Chang, H. L.; Su, W. C.; Wu, T. M.; Jeng, R. J. Polyurethane elastomers through multi-hydrogen-bonded association of dendritic structures. *Polymers* **2005**, *46* (25), 11849–11857.
- (34) Akram, N.; Saleem, S.; Zia, K. M.; Saeed, M.; Usman, M.; Maqsood, S.; Mumtaz, N.; Khan, W. G.; Hafiz-Ur-Rehman. Stoichiometric-architectural impact on thermo-mechanical and morphological behavior of segmented Polyurethane elastomers. *J. Polym. Res.* **2021**, *28* (7), 238.
- (35) Quirino, R. L.; Da Silva, T. F.; Payne, A.; de V V Lopes, R.; Paterno, L. G.; Sales, M. Synthesis and thermomechanical properties of polyurethanes and biocomposites derived from macauba oil and coconut husk fibers. *Coatings* **2015**, *5* (3), 527–544.
- (36) Akram, N.; Gurney, R. S.; Zuber, M.; Ishaq, M.; Keddie, J. Influence of Polyol Molecular Weight and Type on the Tack and Peel Properties of Waterborne Polyurethane Pressure-Sensitive Adhesives. *Macromol. React. Eng.* **2013**, *7* (10), 493–503.
- (37) Afifi, M.; El-Naggar, M. E.; Muhammad, S.; Alghamdi, N. A.; Wageh, S.; Abu-Saied, M.; El-Morsy, M.; Salem, W. M.; Mostafa, M. S.; Salem, S. R.; et al. Chemical stability, morphological behavior of Mg/Sr-hydroxyapatite@ chitosan biocomposites for medical applications. *J. Mater. Res. Technol.* **2022**, *18*, 681–692.
- (38) Trakoolwannachai, V.; Kheolamai, P.; Ummartyotin, S. Characterization of hydroxyapatite from eggshell waste and polycaprolactone (PCL) composite for scaffold material. *Composites, Part B* **2019**, *173*, 106974.
- (39) Timpu, D.; Sacarescu, L.; Vasiliu, T.; Dinu, M. V.; David, G. Surface cationic functionalized nano-hydroxyapatite-preparation, characterization, effect of coverage on properties and related applications. *Eur. Polym. J.* **2020**, *132*, 109759.
- (40) Patil, A. M.; Jirimali, H. D.; Jagtap, R. N. Study of coating performance of bio-based hyperbranched polyester polyol/graphene oxide composites in PU-coating. *J. Macromol. Sci.* **2020**, *58* (2), 81–89.
- (41) El Kaim Billah, R.; Zaghoul, A.; Ahsaine, H. A.; BaQais, A.; Khadoudi, I.; El Messaoudi, N.; Agunaou, M.; Soufiane, A.; Jugade, R. Methyl orange adsorption studies on glutaraldehyde cross-linking chitosan/fluorapatite-based natural phosphate composite. *Int. J. Environ. Anal. Chem.* **2022**, 1–17.
- (42) Radoor, S.; Karayil, J.; Jayakumar, A.; Parameswaranpillai, J.; Siengchin, S. J. C.; Physicochemical, S. A.; Aspects, E. Efficient removal of methyl orange from aqueous solution using mesoporous ZSM-5 zeolite: Synthesis, kinetics and isotherm studies. *Colloids Surf., A* **2021**, *611*, 125852.
- (43) Sriram, G.; Bendre, A.; Altalhi, T.; Jung, H.-Y.; Hegde, G.; Kurkuri, M. Surface engineering of silica based materials with Ni-Fe layered double hydroxide for the efficient removal of methyl orange: Isotherms, kinetics, mechanism and high selectivity studies. *Chemosphere* **2022**, *287*, 131976.
- (44) Akartasse, N.; Azzaoui, K.; Mejdoubi, E.; Hammouti, B.; Elansari, L. L.; Abou-Salama, M.; Aaddouz, M.; Sabbahi, R.; Rhazi, L.; Siaj, M. Environmental-friendly adsorbent composite based on hydroxyapatite/hydroxypropyl methyl-cellulose for removal of cationic dyes from an aqueous solution. *Polymers* **2022**, *14* (11), 2147.